International Journal of Nanomedicine

Dovepress
open access to scientific and medical research

Open Access Full Text Article

ORIGINAL RESEARCH

Polycaprolactone/maltodextrin nanocarrier for intracellular drug delivery: formulation, uptake mechanism, internalization kinetics, and subcellular localization

This article was published in the following Dove Press journal:
International Journal of Nanomedicine
29 July 2015
Number of times this article has been viewed

Maxwell Korang-Yeboah[1]
Yamini Gorantla[1]
Simon A Paulos[1]
Pankaj Sharma[2]
Jaideep Chaudhary[2]
Ravi Palaniappan[1]

[1]Department of Pharmaceutical Sciences, College of Pharmacy and Health Sciences, Mercer University, [2]Center for Cancer Research and Therapeutic Development (CCRTD), Clark Atlanta University, Atlanta, GA, USA

Abstract: Prostate cancer (PCa) disease progression is associated with significant changes in intracellular and extracellular proteins, intracellular signaling mechanism, and cancer cell phenotype. These changes may have direct impact on the cellular interactions with nanocarriers; hence, there is the need for a much-detailed understanding, as nanocarrier cellular internalization and intracellular sorting mechanism correlate directly with bioavailability and clinical efficacy. In this study, we report the differences in the rate and mechanism of cellular internalization of a biocompatible polycaprolactone (PCL)/maltodextrin (MD) nanocarrier system for intracellular drug delivery in LNCaP, PC3, and DU145 PCa cell lines. PCL/MD nanocarriers were designed and characterized. PCL/MD nanocarriers significantly increased the intracellular concentration of coumarin-6 and fluorescein isothiocyanate-labeled bovine serum albumin, a model hydrophobic and large molecule, respectively. Fluorescence microscopy and flow cytometry analysis revealed rapid internalization of the nanocarrier. The extent of nanocarrier cellular internalization correlated directly with cell line aggressiveness. PCL/MD internalization was highest in PC3 followed by DU145 and LNCaP, respectively. Uptake in all PCa cell lines was metabolically dependent. Extraction of endogenous cholesterol by methyl-β-cyclodextrin reduced uptake by 75%±4.53% in PC3, 64%±6.01% in LNCaP, and 50%±4.50% in DU145, indicating the involvement of endogenous cholesterol in cellular internalization. Internalization of the nanocarrier in LNCaP was mediated mainly by macropinocytosis and clathrin-independent pathways, while internalization in PC3 and DU145 involved clathrin-mediated endocytosis, clathrin-independent pathways, and macropinocytosis. Fluorescence microscopy showed a very diffused and non-compartmentalized subcellular localization of the PCL/MD nanocarriers with possible intranuclear localization and minor colocalization in the lysosomes with time.

Keywords: endocytosis, prostate cancer, subcellular targeting, macropinocytosis, clathrin-mediated endocytosis

Introduction

Polymeric nanocarriers have generated much interest and attention due to their amenable properties, such as ease of surface modification, ideal size range, biocompatibility, and biodegradability, which allow them to be employed in numerous fields of medicine.[1–3] In cancer therapeutics, polymeric nanocarriers offer the added advantage of specific organ and subcellular targeting either into the cytoplasm, nucleus, or other specialized organelles. This makes polymeric nanocarriers ideal candidates for the subdelivery of both bio- and chemotherapeutic agents as they enhance clinical efficacy while minimizing the incidence of side effects.[3,4] However, at the heart of

Correspondence: Ravi Palaniappan
Department of Pharmaceutical Sciences, College of Pharmacy and Health Sciences, Mercer University, 3001 Mercer University Drive, Atlanta, GA 30341, USA
Tel +1 678 547 6239
Fax +1 678 547 6423
Email palaniappan_r@mercer.edu

this is a series of biological events that take place, including interactions between the drug carriers and cellular structures as well as trafficking mechanisms that require a much-detailed understanding.

A thorough understanding of the various interactions between cellular structures and nanoparticles is key in designing efficient drug carrier systems due to the direct correlation that exists between cellular uptake, intracellular trafficking mechanism and drug bioavailability, clinical efficacy, and therapeutic outcome of the entrapped active drug.[5,6] However, there seems to be a lack of in-depth understanding of how to effectively optimize intracellular delivery because cellular uptake mechanisms and rates vary widely with the type, size, charge, and surface properties of the nanoparticles employed, and more importantly, with the cell type under study.[6–9] This, hence, makes it implausible for broad generalizations to be made, and there is therefore the need to treat each nanocarrier and cell type specifically on a case-to-case basis. In addition, the rate of cellular uptake varies with cell population density,[10,11] further making it very challenging to draw general conclusions for the enhancement of particle cellular uptake. Noteworthily, the uptake, trafficking, and localization of quantum dots have been reported to vary in three subclones of the same cell type, thus illustrating the importance of the cell phenotype on cellular uptake.[12]

Polycaprolactone (PCL) is one of the most widely employed polymers for subcellular drug delivery and tissue engineering. PCL is an United States Food and Drugs Administration (FDA)-approved biodegradable, biocompatible, and semicrystalline polyester.[13–15] Its hydrophobic nature promotes efficient cellular uptake.[16–18] Unlike polyglycolide and poly(D,L-lactide) and its copolymers, PCL degrades at a much slower rate, allowing sustained delivery of encapsulated proteins and protection from acidic degradants.[13] It is therefore a better candidate for the delivery of peptides and proteins and for the induction of a more sustained drug release profile. However, very little to nothing is known of the uptake mechanisms and subcellular localization of PCL-based nanoformulations in PCa cell lines. Maltodextrin (MD), on the other hand, is a food additive generally considered safe by the FDA, and is used as a lyoprotectant in pharmaceutical formulations.[19] Corveleyn and Remon have demonstrated the superiority of MD to sucrose as a lyoprotectant during freeze drying of lactate dehydrogenase.[19] Additionally, MD has a protective effect similar to sucrose in stabilizing chymopapain and maintaining the enzymatic activity of chymopapain for 3 years at room temperature.[20] Furthermore, earlier work by our lab has demonstrated the robust nature and usefulness of MD in protecting encapsulated protein from the harsh process conditions during formulation.[21]

One such area for the application of polymeric nanoparticle intracellular delivery of active therapeutics is the targeting and killing of cancer cells, commonly of the prostate, breast, bladder, and pancreas. Prostate cancer (PCa) remains the most common form of malignancy in men and is the second highest cause of deaths from cancer in men, the first being lung cancer. PCa is characterized by a high degree of heterogeneity and exhibits pronounced biological, hormonal, and molecular complexities.[22,23] While the impact of these complexities on drug treatment is well studied, their possible impact on biological interactions responsible for cellular uptake and localization of nanocarriers remains unexploited. Also, disease progression and metastasis are associated with significant genetic and phenotypic alterations that contribute to the changes observed in cell surface polarity, intracellular and extracellular protein expressions, and cell phenotype. These events may modify nanocarrier uptake kinetics, sorting mechanism, and subcellular localization.[24,25]

The purpose of this study was therefore to evaluate the impact of PCa cell phenotype and disease progression on the cellular internalization of a PCL-based nanoformulation. The study reports the development of a polymeric vector for intracellular drug delivery and further evaluates the kinetics and mechanisms of its internalization as well as its subcellular localization in LNCaP, DU145, and PC3 PCa cell lines. These cell lines are the most studied cellular models and represent most of the phenotypic changes that occur during progression of the disease.[26] LNCaP has a high expression in the androgen receptor (AR) and is androgen sensitive, a characteristic of the early phase of the cancer. As the cancer progresses, it becomes more androgen insensitive, more aggressive, and fails to respond to androgen deprivation therapy, a condition referred to as castration-resistant PCa. DU145 and PC3 are androgen insensitive and exhibit bone metastatic behavior and are osteolytic.[27] Additionally, these cell lines are known to exhibit marked differences in terms of their tumorigenicity. LNCaP, however, has very low levels of tumorigenicity, while DU145 and PC3 are moderately and highly tumorigenic, respectively.

Materials and methods

Materials

All cell lines (LNCaP, DU145, PC3, WPE1-NA22) were purchased from American Type Culture Collection (ATCC) (Manassas, VA, USA). MD was purchased from Grain Processing Corporation (Muscatine, IA, USA). PCL (MW =80,000 g/mol) and methylene chloride, polyvinyl alcohol, methyl-β-cyclodextrin (MβCD), and nystatin were purchased from Thermo Fisher Scientific (Waltham, MA, USA). Amiloride was purchased from Tocris Bioscience (Bristol, UK),

chlorpromazine (CPZ) was purchased from Enzo Life Sciences (Farmingdale, NY, USA), and coumarin was purchased from Acros Organics (Thermo Fisher Scientific). RPMI-1640 medium, F-12 medium, penicillin–streptomycin, fetal bovine serum, and LysoTracker Red™ were purchased from Gibco® Invitrogen Corporation (Grand Island, NY, USA).

Methods

Formulation of PCL/MD nanocarrier

PCL/MD nanoparticles were formulated by double-emulsion solvent technique with some modifications. Briefly, about 5 mg of fluorescein isothiocyanate-labeled bovine serum albumin (FITC-BSA) dissolved in 1 mL of aqueous MD solution was emulsified with 50 mg of PCL in 6 mL of methylene chloride. The resulting primary emulsion was further homogenized in 50 mL of a 2% polyvinyl alcohol solution using the Nano DeBEE high pressure homogenizer at single passage of 10,000 psi to produce a w/o/w emulsion. Removal of the organic phase resulted in coacervation of PCL to yield a nanosuspension. The nanoparticles were isolated by centrifugation, washed at least three times to remove any residual organic solvent, and freeze dried for further studies. To prepare coumarin-loaded nanoparticles, 50 µg of coumarin was added to the organic phase and subjected to the same processes as noted above.

Physicochemical characterization of nanocarrier

Particle size and size distribution (polydispersity index [PDI]) were determined by dynamic light scattering using a Malvern Zetasizer (Malvern Instruments, Malvern, UK). The freeze-dried nanoparticles were dispersed in filtered deionized water for size measurements. The particle size was expressed as volume mean diameter. To determine the electrophoretic mobility or zeta potential, the particles were redispersed in 0.9% NaCl solution. The particle size, zeta potential, and PDI results were reported as the mean of at least three determinations ± standard deviation. The efficiency of entrapment of the nanoformulation was evaluated with BSA as a model large molecule using the equation:

$$\text{Entrapment efficiency (\%)} = \frac{\text{Weight of drug in PCL/MD NPs}}{\text{Weight of feeding drug}} \times 100$$

Differential scanning calorimetry analysis

Differential scanning calorimetry analysis was conducted using DSC Q100 from TA Instruments, previously standardized using the melting point of indium. About 5 mg of lyophilized nanocarrier, PCL and 10 mg of MD samples were analyzed individually in a hermetically sealed aluminum pan. The samples were scanned at a rate of 5°C/min from 0°C to 300°C. The scans were conducted as triplicates for each sample to ensure reproducibility.

Effect of increasing MD content on nanocarrier release of encapsulated protein

The effect of increasing the content of MD on the in vitro release of BSA was determined in phosphate-buffered saline (PBS) at a pH of 7.4. Separate vials containing the lyophilized nanocarrier (with different amounts of MD) dissolved in PBS were incubated at 37°C under continuous shaking at 200 rpm. The contents of the vials were withdrawn at separate time points, centrifuged at 30,000 *g*, and the supernatant was analyzed for the protein content using the Pierce micro bicinchoninic acid assay (n=3).

Cell culture

The nontumorigenic, human prostate epithelial cell line WPE1-NA22 was maintained in Keratinocyte-SFM (1X) medium supplemented with prequalified human recombinant epidermal growth factor and bovine pituitary extract. PC3 and LNCap PCa cell lines were maintained in RPMI-1640 supplemented with 10% fetal bovine serum, 2 mM L-glutamate, 1% penicillin–streptomycin in a humidified chamber at 37°C, and 5% CO_2. DU145 PCa cell line was cultured in complete Ham's F-12 medium. For microscopic imaging, the cells were seeded on sterile 15 mm collagen-treated glass coverslips in six-well plates and allowed to grow to about 50%–70% confluency.

In vitro cell viability assay

The cytocompatibility of PCL/MD nanocarrier with normal, nontumorigenic human cell lines was evaluated in WPE1-NA22 cells using CellTiter 96® AQueous Non-Radioactive Cell Proliferation Assay from Promega Corporation. About 1×10^4 cells/well were seeded overnight in a 96-well plate. Samples of the nanocarrier of concentration range 1–10 mg/mL were added and incubated for 24 hours at 37°C and 5% CO_2. The medium was replaced; 20 µL of combined [3-(4,5-dimethylthiazol-2-yl)-5-(3-carboxymethoxyphenyl)-2-(4-sulfophenyl)-2H-tetrazolium (MTS) phenazine methosulfate (PMS) (333 µg/mL MTS and 25 µM PMS) solution per 100 µL culture medium was added and incubated for 2 hours at 37°C. The absorbance at 490 nm, which corresponds to the number of viable cells, was recorded and from that the percentage cell viability was computed using the nontreated group as control. The percentage of cell viability was determined using the equation: (average absorbance ×100)/control absorbance. The experiment was also performed for the three PCa cell lines.

Flow cytometry analysis of internalization and uptake kinetics

The efficiency of the intracellular drug delivery of the PCL/MD nanocarrier was evaluated by flow cytometry (BD Accuri™ C6 flow cytometer). The nanocarrier was fluorescently labeled with FITC-BSA or coumarin-6 dye as model drug molecules. The cell lines were plated at a concentration of about 1.0×10^6 cells/well in a six-well plate overnight. Each cell line (DU145, PC3, and LNCap) was then incubated for 2 hours with 25 μg/mL of fluorescently labeled nanoparticles, free drug and the third group was left untreated to serve as a control. The cell lines were washed at least three times with Hanks' balanced salt solution (HBSS) to remove any attached nanocarrier, detached, and brought to a single cell suspension for cytometric analysis. Each cell population was gated to remove any debris, free nanoparticles, or dead cells. Shifts in the fluorescence peaks were monitored with 10,000 live cells per group in the gated population of live cells using the FL1 filter for our fluorophore. A shift in the peak from that observed at t=0 indicated cellular uptake. In order to eliminate any false positives arising from the leakage of dye from the nanocarriers, another control experiment was conducted with a medium in which 25 μg/mL of fluorescently labeled nanocarriers were suspended for at least 2 hours. The medium was centrifuged, and the cells were then incubated for 2 hours with the supernatant. The kinetics of uptake was also studied by flow cytometry for a 12-hour period. The mean fluorescence peak intensity, which correlates directly with the amount of nanoparticles engulfed, was used as an indirect measure of the nanoparticle uptake. The basal fluorescence peak of the cells was taken into account for the final computed values. Data acquisition and analyses were conducted with the Accuri™ C6 flow cytometer software.

Fluorescence microscopic colocalization studies

Uptake and subcellular localization of the nanocarrier was confirmed using fluorescence microscopy with a Zeiss Axio Imager Z1 ApoTome microscope. The nanoparticles were loaded with the fluorophore coumarin-6 to aid in their visualization. The cells were then incubated for 5 minutes, 30 minutes, 1 hour, 2 hours, 6 hours, and 12 hours with 25 μg/mL of PCL/MD nanoparticles diluted with RPMI or F-12 serum-free medium. The cells were washed three times with HBSS and stained with LysoTracker® Red DND-99 (excitation/emission: 577/590 nm), a red-fluorescent dye for the specific labeling of acidic organelles in live cells for 30 minutes. The cells were fixed with 4% paraformaldehyde in PBS (pH 7.4), followed by nuclear staining with ProLong® Gold antifade reagent with DAPI (4′,6-diamidino-2-phenylindole) (excitation/emission: 358/461 nm). Microscopic images were then taken using three different filters.

Cellular uptake mechanism of PCL/MD nanocarrier

To evaluate the pathways utilized by the nanocarriers for cellular uptake, several endocytic pathways were excluded using a variety of pharmacological inhibitors. Table 1 shows the agents used, their various concentrations applied, the treatment period undertaken, and the specific pathways they exclude. The cell lines were exposed to the agents before treatment with the PCL/MD nanocarriers for 2 hours. The cell lines were then washed at least three times with HBSS and analyzed using flow cytometry. Changes in the fluorescence intensity were expressed as a percentage of the control group (no pharmacological inhibitor used). The effect of cellular metabolism on cellular uptake PCL/MD nanocarrier was assessed by incubating all cell lines at 4°C prior to and during treatment with the nanocarriers. PC3, LNCaP, and DU145 cells were treated for 30 minutes with coumarin-loaded nanocarrier at either 37°C or 4°C, and the mean fluorescence intensities corresponding to cellular uptake were quantified using flow cytometry.

Statistical analysis

Data for physicochemical characterization and internalization studies represent the mean ± standard deviation of at least three independent determinations. Statistical analyses

Table 1 Endocytic pathways, pharmacological inhibitors, treatment concentration, and duration used in this study

Endocytic inhibitor	Concentration/duration of exposure	Mechanisms affected
Sodium azide	0.1% for 45 min	ATP inhibitor
CPZ	10 μg/mL, 1 hr at 37°C	CME
Nystatin	20 μg/mL for 45 min at 37°C	CIE
MβCD	5 mM for 1 hr at 37°C	Cholesterol-dependent-macropinocytosis, CME, and CIE giving rise to small vesicles
Amiloride	50 μM for 45 min	Macropinocytosis

Abbreviations: min, minutes; ATP, adenosine triphosphate; CPZ, chlorpromazine; hr, hours; CME, clathrin-mediated endocytosis; CIE, clathrin-independent endocytosis; MβCD, methyl-β-cyclodextrin.

for comparison between two groups and among multiple groups and control groups were carried out using Student's *t*-test and one-way analysis of variance, respectively, at a *P*-value of 0.05.

Results

The nanocarriers were of average particle size of 170 nm (range of 120–220 nm) (Figure 1) with low polydispersity. Encapsulation of BSA or coumarin did not significantly alter the mean size, size range, or polydispersity. The zeta potential, an indicator of colloidal stability, was moderately low (Table 2). The nanoformulation had high encapsulation efficiency and yield. The formulation design consistently yielded more than 98% of the initial mass of solid matter used, and about 80% (78.83%±7.40%) of the initial BSA concentration used was encapsulated (Table 2). The encapsulation efficiency of the nanoformulation was significantly higher when a model small molecule was entrapped. Using coumarin-6 as a model small molecule, the encapsulation efficiency obtained was greater than 90%.

The thermal behaviors of MD, PCL, and the nanocarriers were studied using differential scanning calorimetry (Figure 2). A single, sharp melting point peak at 62.09°C was obtained for PCL, and two very broad amorphous peaks from 37.5°C to 125°C and 225°C to 250°C were obtained for MD. The lyophilized nanocarrier, however, showed a single endothermic peak, which shifted slightly to the left with a peak temperature of about 56.43°C but showed none of the two broad peaks for MD.

In a previous study we evaluated the impact of the dextrose equivalent of MD on the stability of an encapsulated protein. In this study, however, we proceeded further to investigate the impact of varying amounts of MD on the release profile of encapsulated BSA. We observed that the total amount of protein released increased significantly ($P<0.05$) from about 25.47%±3.45% (no MD) to 81%±4.24% (100 mg MD) over 7 days (Figure 3) with an increase in the amount of MD added. There was, however, no significant effect on the initial drug burst release observed.

Further, the nanocarrier showed significant ($P<0.05$) biocompatibility with normal prostate epithelial cells (WPE1-NA22) at the concentration range studied (Figure 4A). The maximum level of toxicity was observed at the highest dose studied (10 mg/mL) after 48 hours and 72 hours of exposure, which resulted in about 23% and 27% decrease in cell viability, respectively. Also, the uptake of the nanoparticles did not significantly affect the viability of PC3, LNCaP, and DU145 PCa cell lines over the studied concentration range of 1–10 mg/mL when compared to the controls (no treatment and dimethyl sulfoxide treatment) (Figure 4B). The maximum decrease in the cell viability was observed at the highest concentration used (10 mg/mL), which was far in excess of the dose utilized in internalization studies (25 µg/mL), indicating that changes in the cellular uptake could not be attributed to a decrease in the cell viability.

As shown in Figure 5, all three cell lines internalized the PCL/MD nanocarrier, and the nanocarrier demonstrated a significantly higher bioavailability in comparison with the administration of the free coumarin-6 dye. A similar result was obtained when FITC-BSA was used in place of coumarin-6. The shift in peak ranged from a single logarithmic fold change observed in LNCaP to as high as two logarithmic units change in intensity as seen in PC3. The cells were washed at least three times in PBS (pH 7.4) to eliminate any effect contributed by the adsorbed dye or nanoparticles.

The effect of the duration of incubation on cellular internalization was also investigated over a 12-hour period

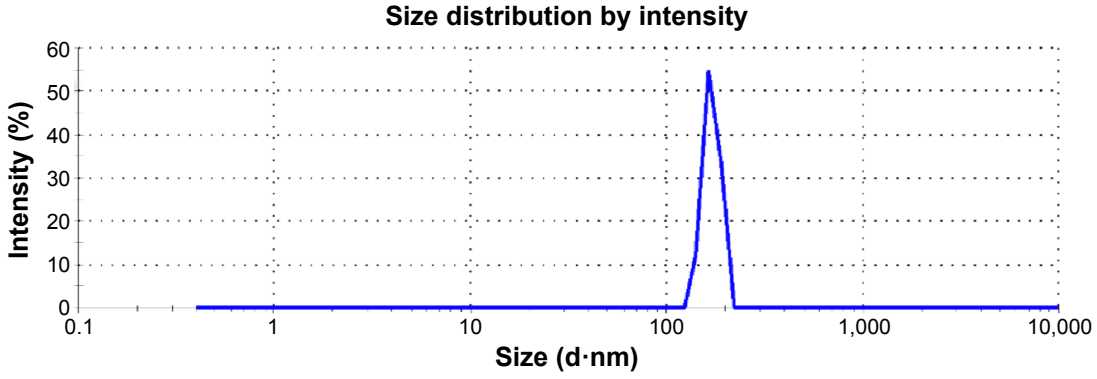

Figure 1 PCL/MD nanocarrier size distribution by intensity.
Abbreviations: PCL, polycaprolactone; MD, maltodextrin.

Table 2 Physicochemical characteristics of PCL/MD nanocarrier

Average size (range)	170 nm (120–220 nm)
Polydispersity index	0.11±0.04
Zeta potential	–8.30 mV
Encapsulation efficiency	78.83%±7.40%
Percentage yield	>98%

Note: Data are presented as mean ± standard deviation for polydispersity index and encapsulation efficiency.
Abbreviations: PCL, polycaprolactone; MD, maltodextrin.

using flow cytometry to gain further understanding of the kinetics of the cellular uptake of the nanocarriers. Since the mean fluorescence of the untreated cells was not different from fluorescence due to possible leakage of the dye during the period of study or that of the blank nanocarrier, any changes in the mean fluorescence was attributed to that of an internalized labeled nanocarrier. A change in the mean fluorescence therefore correlated directly with changes in the cellular internalization. All the three PCa cell lines internalized the nanocarrier within the first 5 minutes of the experiment (Figure 6). The rate of cellular uptake of the nanocarriers was initially high during the first hour post-incubation but decreased to an almost constant rate in PC3 and DU145 for the rest of the duration of the study. LNCaP showed a similar pattern during the first 2 hours of study but showed a decrease in the mean fluorescence intensity after 2 hours with no significant change in the uptake from the sixth to 12th hour. Overall, PC3 exhibited the highest nanocarrier internalization followed by DU145 and then LNCaP. Importantly, the calculated area under the curve (AUC) for the PC3 kinetic plot was about 2- and 1.3-fold higher than LNCaP and DU145 PCa cell lines, respectively.

The results of the colocalization study supported the uptake kinetics studies of PCL/MD (Figure 7A–G). Upon initial exposure, much of the nanocarrier was seen adhering to the cellular membrane. The amount of subcellular nanocarriers however increased with time with possible intranuclear localization obtained. Colocalization with the lysosomes was also observed especially within the first hour, although the majority of the fluorescence signal was emitted from other cytoplasmic organelles other than the lysosome (Figures S2 and S3).

Noteworthily, all the PCa cell lines showed significant ($P<0.05$) decrease in the cellular uptake of PCL/MD nanocarriers by about 60%–80% when treated at 4°C compared to treatment at 37°C (Figure 8A). However, the nanocarrier-treated cell lines at 4°C still showed higher uptake in comparison to the untreated group. The results were further confirmed with the pretreatment of the cells with sodium azide, a metabolic/ATP inhibitor (Figure 8B). Cellular uptake in all cell lines decreased by 50%–60% upon metabolic inhibition with sodium azide.

Further, cellular uptake and internalization route usually determine the intracellular fate and sorting mechanism of

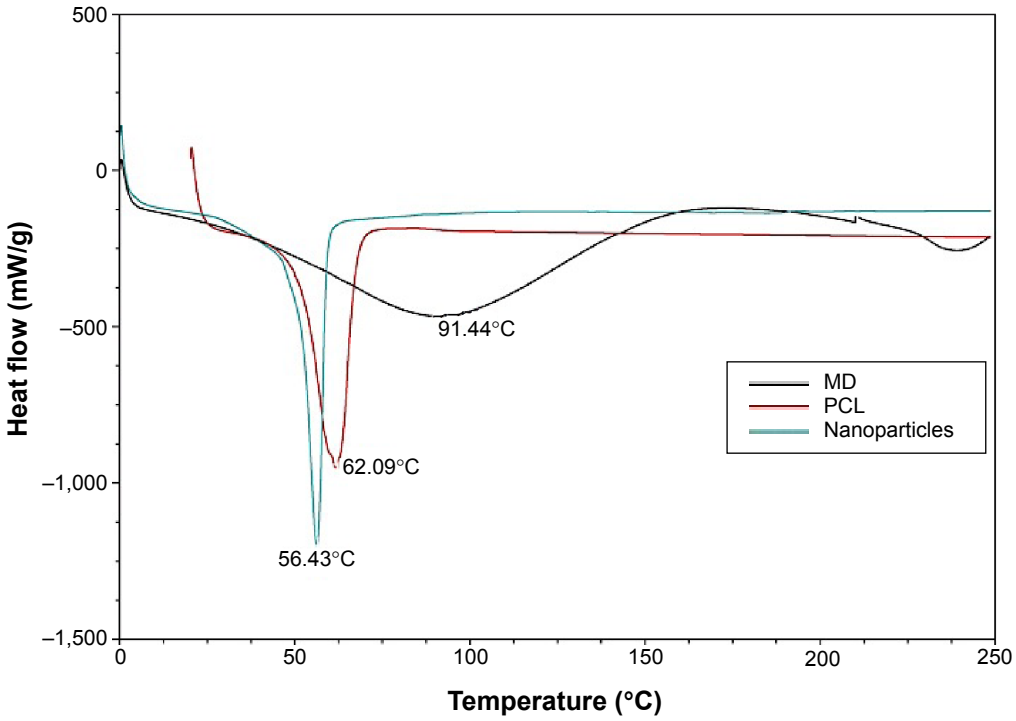

Figure 2 Thermal analysis of MD, PCL, and PCL/MD nanoparticle: thermogram of MD (black), polycaprolactone (red), and PCL/MD nanoparticle (green).
Abbreviations: MD, maltodextrin; PCL, polycaprolactone.

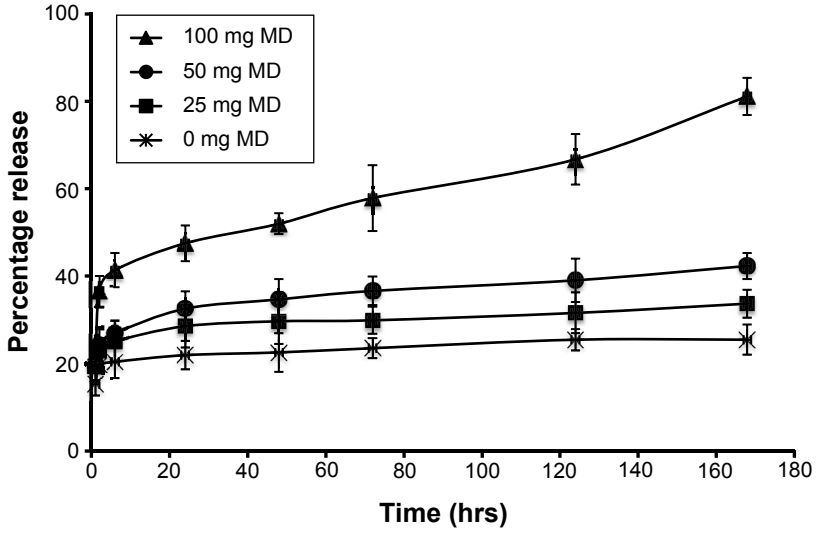

Figure 3 Effect of varying MD content on in vitro release profile of encapsulated BSA.
Abbreviations: MD, maltodextrin; BSA, bovine serum albumin; hrs, hours.

macromolecular carriers. For this reason, we determined the mechanisms involved in the internalization of our nanocarrier. The cells were pretreated with known inhibitors of specific pathways of endocytosis (Table 1), and the changes in the uptake were determined by expressing the mean fluorescence intensity as a relative percentage of the positive control (a nontreated group at 37°C for 2 hours). In order to eliminate false positives, several pharmacological agents were used in this study. The doses of the pharmacological agents utilized were well below minimum toxicity (Figure S1). The role of endogenous cholesterol (involved in macropinocytosis and both clathrin-mediated endocytosis [CME] and clathrin-independent pathways [CIP]) in the cellular uptake of the PCL/MD nanocarrier was explored using MβCD.[28–31] As shown in Figure 9, this resulted in the highest decline of uptake in all the three PCa cell lines studied. There was a 51% decrease in the uptake of PCL/MD nanocarrier in DU145 cell line and about 65% and 75% decrease in LNCaP and PC3 cell lines, respectively. CPZ, a cationic amphiphilic drug, was used to probe the role of clathrin in the uptake of the nanocarrier. CPZ inhibits the formation of clathrin-coated pits through the loss of clathrin and AP2 adaptor complex from the cell surface.[32,33] Clathrin inhibition had a significant ($P<0.05$) effect on nanocarrier internalization in DU145 and PC3 PCa cells but showed minimal effect in LNCaP cell lines (Figure 9). The role of CME in PCL/MD internalization was further confirmed by inhibition with 0.45 M sucrose solution, which inhibits CME by depleting K^+.[34,35]

The role of the CIP was also assessed using nystatin. This resulted in a significant ($P<0.05$) decrease in nanocarrier uptake in all PCa cell lines. Inhibition of CIP decreased PCL/MD internalization by almost 40% in LNCaP and about 29% in PC3. Lastly, pretreatment of the cell lines with amiloride resulted in about 43% decrease in nanocarrier uptake in LNCaP and about 33% and 28% in DU145 and PC3, respectively. Amiloride inhibits macropinocytosis by reducing cytosolic

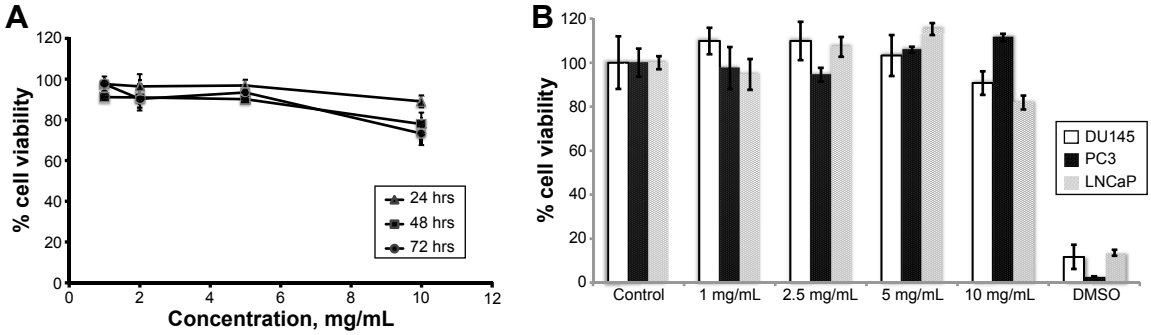

Figure 4 Biocompatibility of PCL/MD nanocarrier.
Notes: (**A**) Effect of blank nanocarrier on the cell viability of normal prostate epithelial cell line WPE1-NA22 (n≥3). (**B**) Cell viability (mean ± SD) of all three cell lines DU145, PC3, and LNCaP after 24 hrs of treatment with increasing nanocarrier concentration (n≥3).
Abbreviations: PCL, polycaprolactone; MD, maltodextrin; SD, standard deviation; hrs, hours; DMSO, dimethyl sulfoxide.

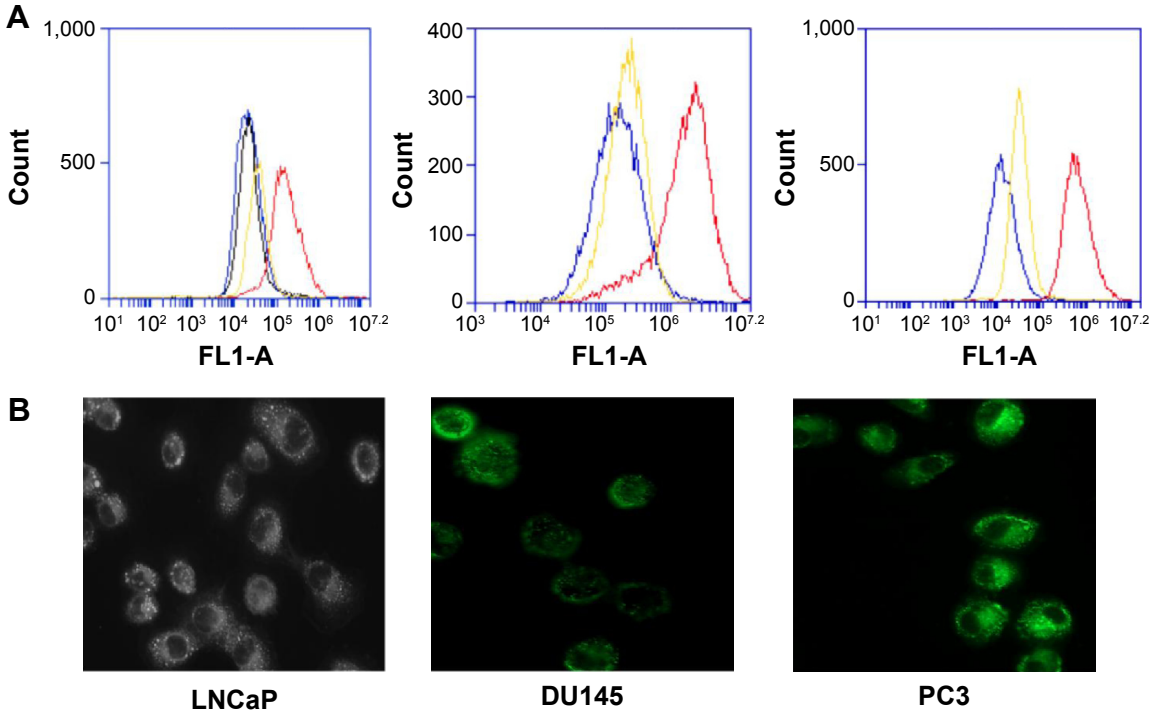

Figure 5 PCL/MD nanocarrier uptake and internalization enhances bioavailability of encapsulated molecule.
Notes: (**A**) Flow cytometry histograms of LNCaP, DU145, and PC3 after 2 hours of treatment with 25 μg/mL of fluorescent-labeled PCL/MD nanocarrier (red), free fluorescent dye (yellow), and untreated cell line (blue) and medium in which an equivalent amount of nanocarrier has been previously suspended (black). (**B**) Cellular internalization of PCL/MD in LNCaP, DU145, and PC3. Fluorescence microscopic images of uptake taken (after 2 hours) with a Zeiss ApoTome microscope with an Axiom Cam version 4.5 imaging system at 40× magnification.
Abbreviations: PCL, polycaprolactone; MD, maltodextrin.

pH and inhibiting Rac1 and Cdc42 signaling.[36,37] The multi-mechanism involved in the cellular uptake thus explained the non-compartmentalized (Figures S2 and S3) and diffused nature of the fluorescence-loaded nanocarrier upon uptake as demonstrated in Figure 9.

Discussion

The unique physicochemical properties of nanocarriers come with several advantages that have been widely exploited in drug delivery and nanotherapeutics. To understand the impact of cancer heterogeneity and disease progression on

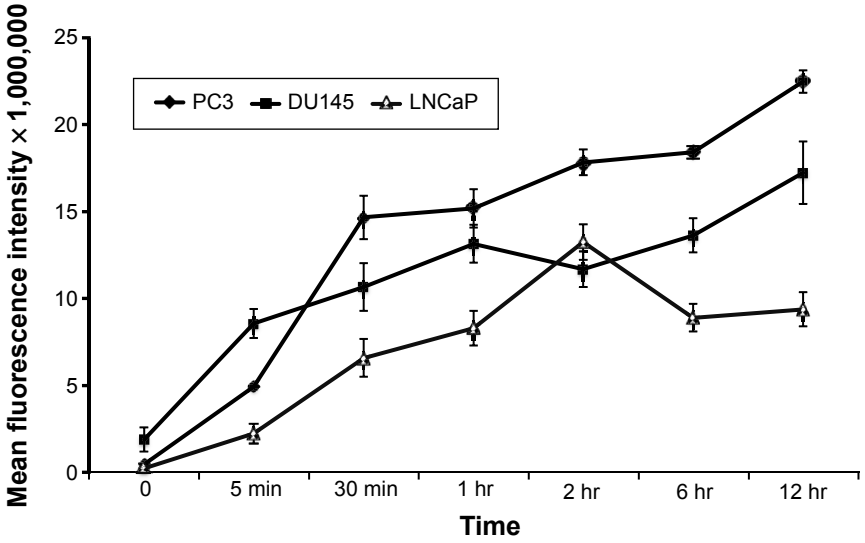

Figure 6 Internalization kinetics of PCL/MD nanoparticles.
Notes: Cells were treated for 5 minutes, 30 minutes, 1 hour, 2 hours, 6 hours, and 12 hours, and analysis was conducted by flow cytometry.
Abbreviations: PCL, polycaprolactone; MD, maltodextrin; min, minutes; hr, hours.

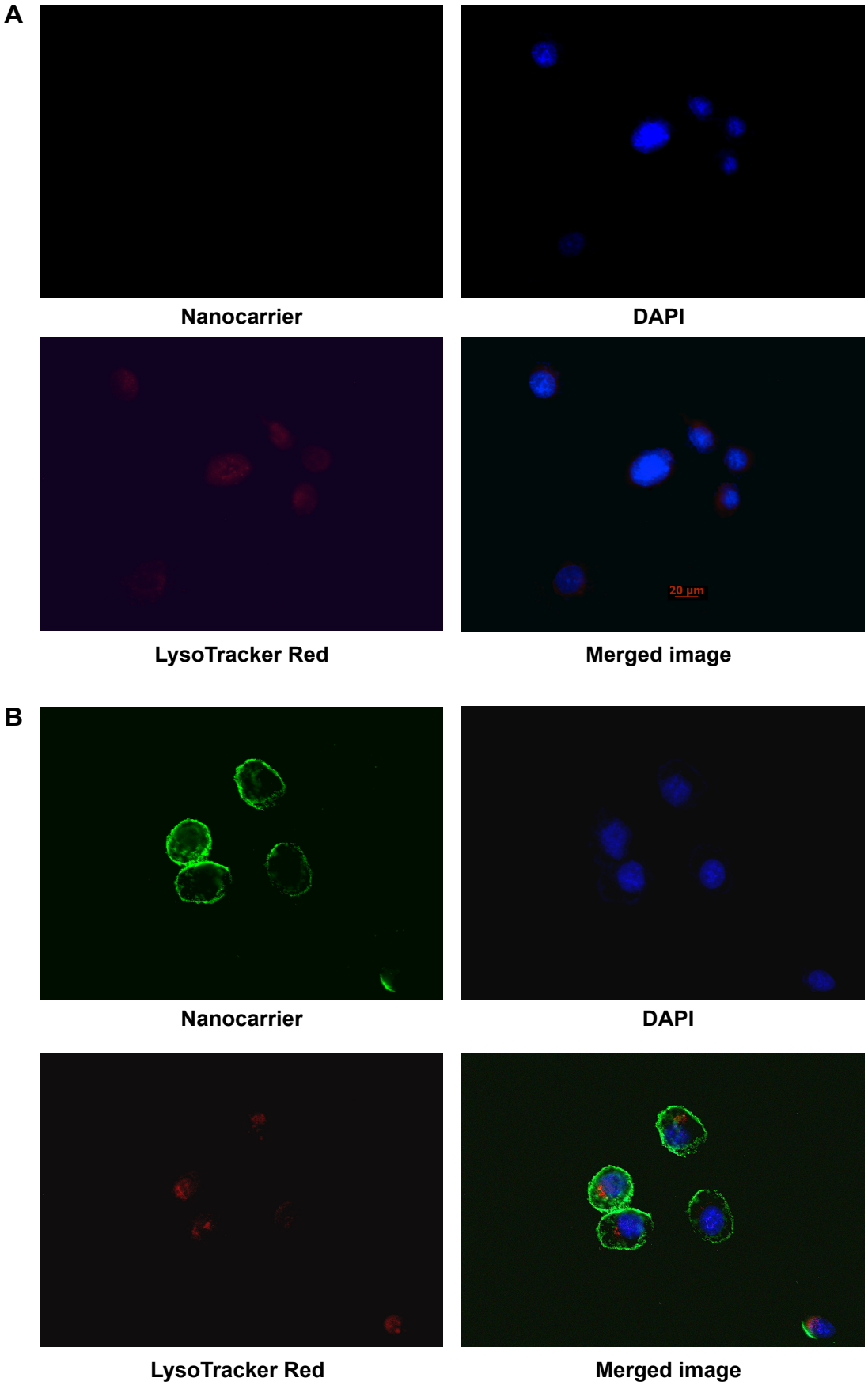

Figure 7 (*Continued*)

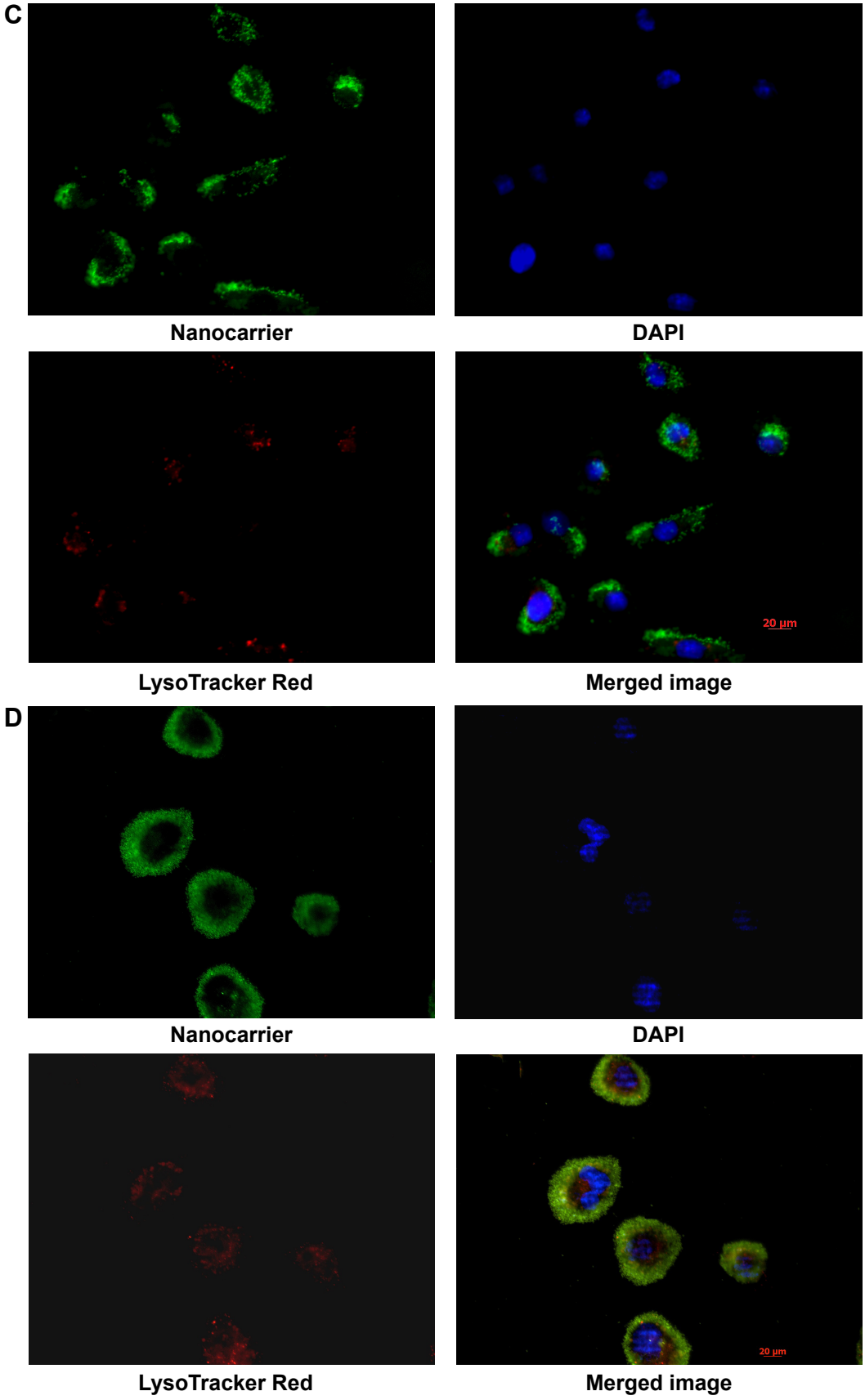

Figure 7 (*Continued*)

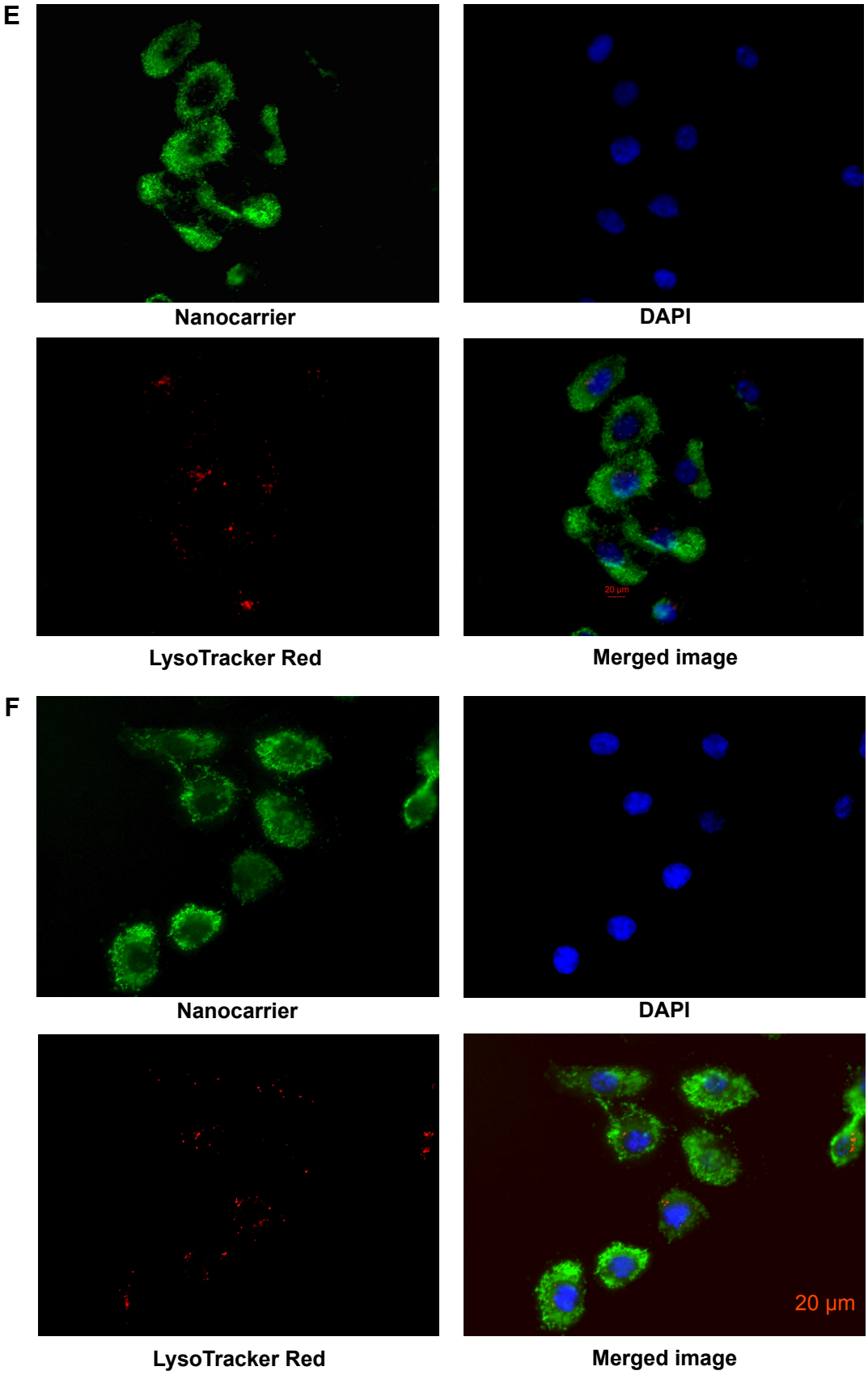

Figure 7 (*Continued*)

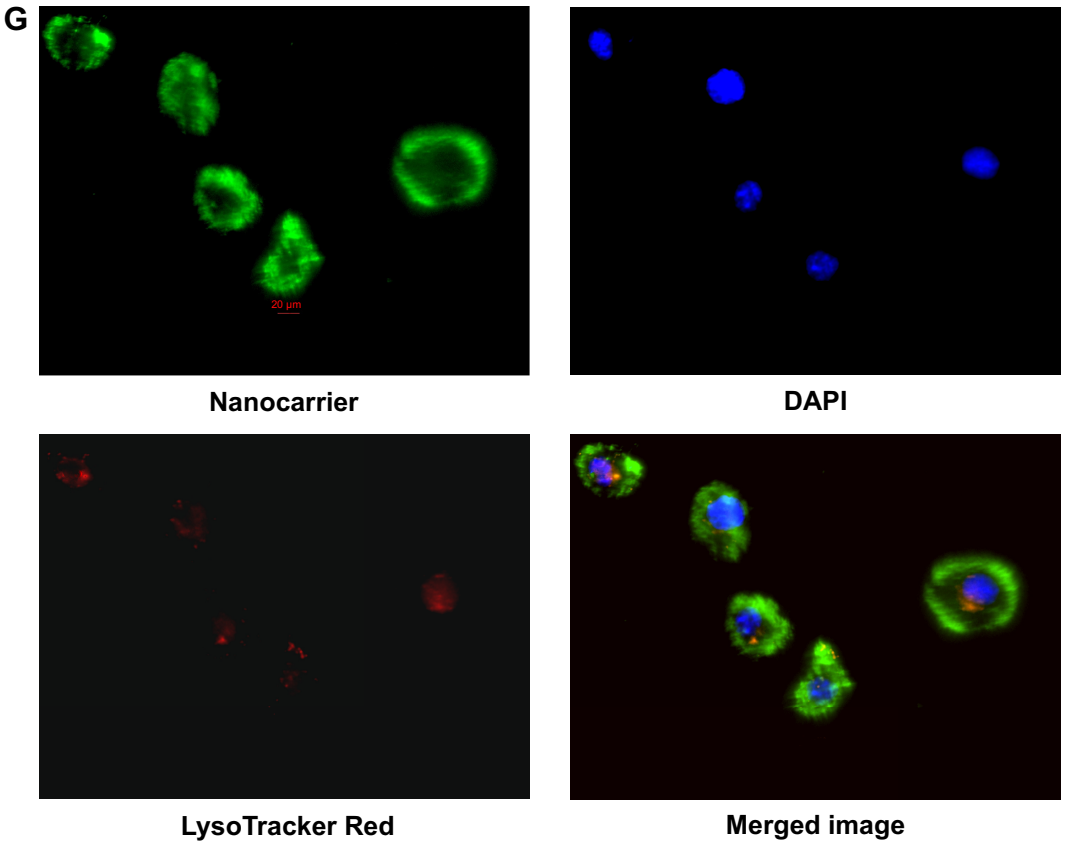

Figure 7 PCL, polycaprolactone; MD, maltodextrin (**A**–**G**) subcellular localization of PCL/MD in PC3 with time (0 minute, 5 minutes, and 30 minutes and 1 hour, 2 hours, 6 hours, and 12 hours): acidic organelles (lysosome-LysoTracker Red), nuclei (DAPI), and cytoplasm in PC3.
Abbreviations: PCL, polycaprolactone; MD, maltodextrin; DAPI, 4′,6-diamidino-2-phenylindole.

nanocarrier interactions with the cancer cells, we employed a PCL-based nanocarrier due to its numerous applications in drug delivery. PCL/MD was designed and characterized accordingly. The double-emulsion technique was employed for formulation development due to its relatively higher encapsulating efficiency for proteins.[38] Particles of average size 170 nm (120–220 nm), narrow PDI, and moderate charge were obtained. Varying the formulation process or components of the nanoformulation did not significantly improve the particle size (data not shown). While there might not be a size limit for cellular entry of particles in the nanometer range, receptor-mediated endocytosis is believed to be predominantly involved in the uptake of particles with size <200 nm and macropinocytosis may be the major route of entry for larger particles.[39–41] Additionally, particles of sizes greater 10 nm but less than 200 nm have been cited to exhibit prolonged circulation and improve bio distribution to tumor cells; hence, they enforce passive drug targeting.[42,43] Further, the illustration of significant ($P<0.05$) high cytocompatibility of both normal prostate epithelial cell lines and PCa cell lines with the nanocarriers can be attributed to the choice of polymers used in the formulation (Figure 4A and B), as both PCL and MD are biocompatible and biodegradable.

Noteworthily, the amount of encapsulated BSA protein released increased substantially as the hydrophilic component (MD) of the formulation was increased.[17,44] The release pattern of encapsulated products in PCL-based nanoformulation has been reported to depend on the properties of both the encapsulated drug and its distribution pattern within the nanocarrier. Hydrophilic agents are mainly dispersed at the interfaces and are usually adsorbed unto the surface of the nanocarrier. The initial drug burst release observed can therefore be attributed to the desorption of the proteins from the surface of the nanocarriers. Also, the sustained release pattern observed of the protein over the period of study has been suggested to be due to particle erosion of the core polymer PCL, which takes weeks to years to degrade extracellularly.[14,17,45]

The DSC analysis of PCL and MD was conducted prior to and after nanoparticle formulation to study the particles' thermal behavior and to identify possible interactions between the excipients. PCL is a semicrystalline polymer that undergoes a first-order endothermic transition at ~60°C. This transition

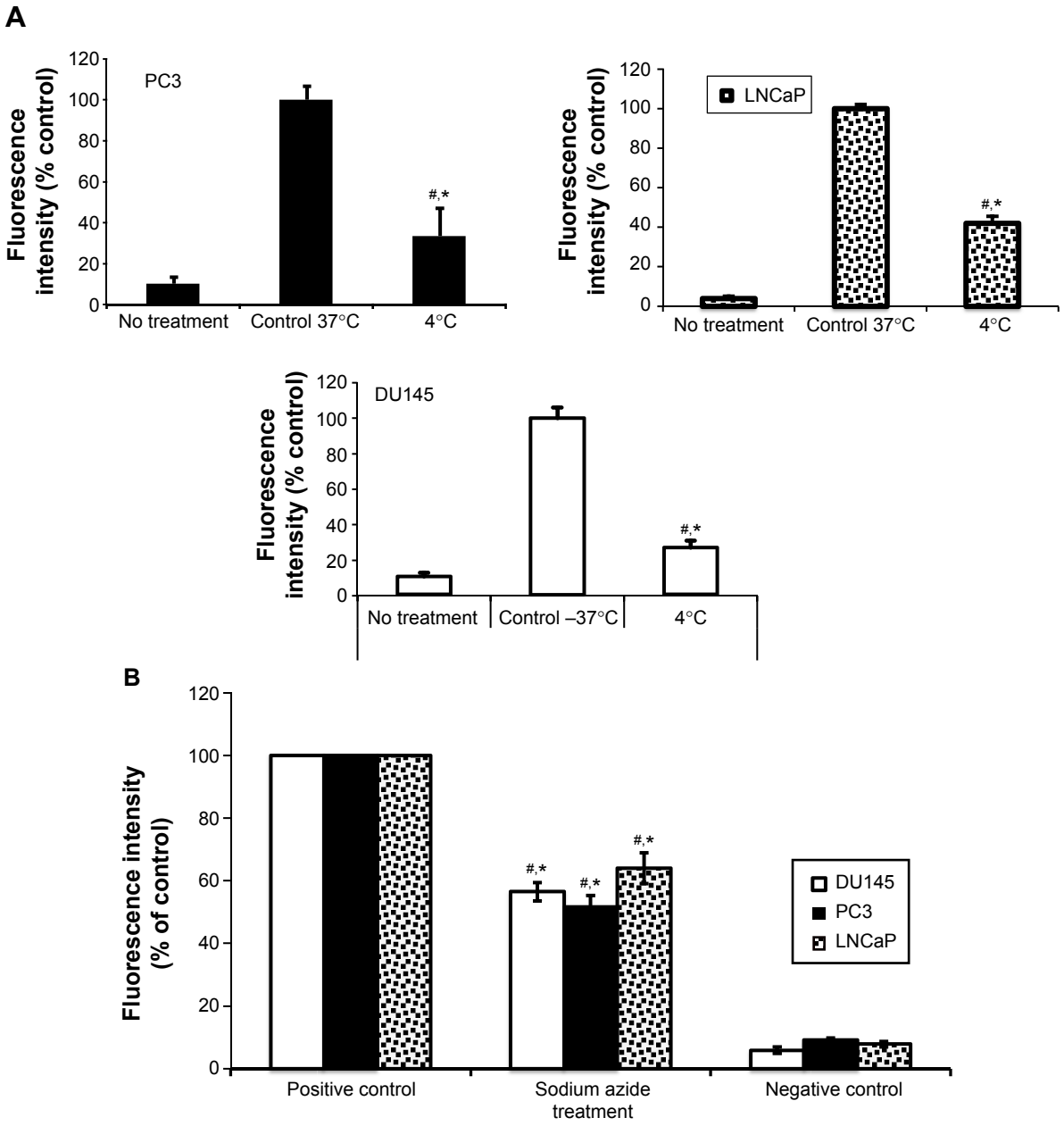

Figure 8 Energy-dependent internalization of PCL/MD in PC3, DU145, and LNCaP (mean fluorescence ± SD).
Notes: (**A**) Cells were treated with 25 μg/mL of fluorescent-labeled nanoparticles at either 37°C or 4°C or untreated (negative control). (**B**) The effect of inhibition of ATP with sodium azide on cellular internalization of PCL/MD nanocarrier in PC3, DU145, and LNCaP. *The treated groups values are significantly less than the positive control, $P<0.05$. #Sodium azide treatment values are significantly higher than the negative controls, $P<0.05$.
Abbreviations: PCL, polycaprolactone; MD, maltodextrin; ATP, adenosine triphosphate; SD, standard deviation.

was observed at ~59.5°C (Figure 2), but a single eutectic melting peak was obtained at ~55°C for the nanoformulation. Even though MD melts at 225°C–250°C, the combination of MD and PCL in our nanoformulation yielded a considerable lower single endothermic peak at ~55°C. The addition of the amorphous MD to the semicrystalline PCL possibly led to a decreased crystallinity in the nanoformulation due to the possible formation of a eutectic mixture. This can hence account for the higher release rate of the encapsulated protein observed after the addition of MD. The first low-intensity broad peak observed in the thermogram of MD corresponds to evaporation of loosely bound water molecules. This peak was absent in the lyophilized nanoformulation due to the loss of bound water upon drying, as suggested by previous studies.[18,46–48]

Nanocarrier internalization and subsequent release of encapsulated product presents a major advantage in the delivery of small molecules where low solubility tends to limit

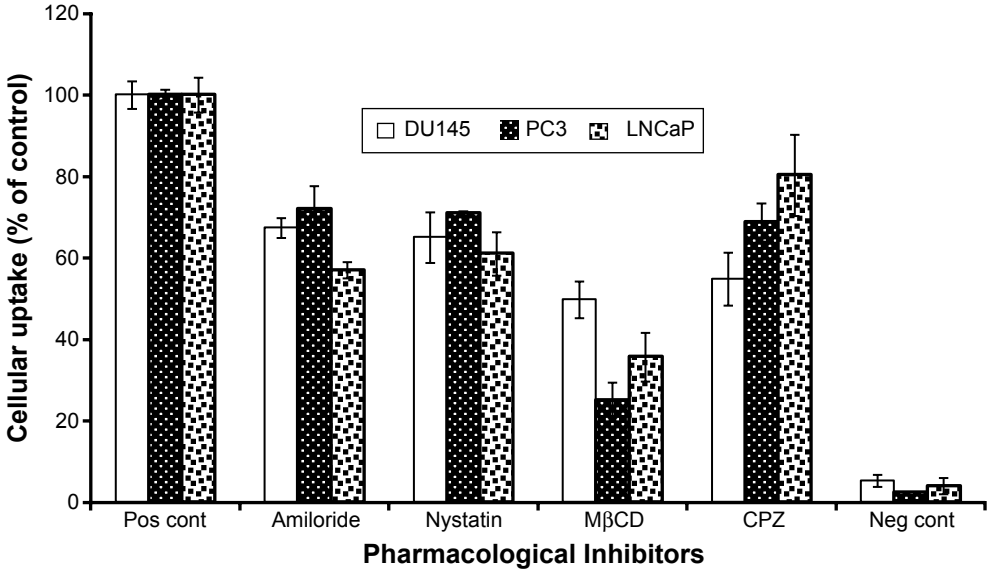

Figure 9 Effect of pharmacological inhibitors on PCL/MD uptake in PC3, DU145, and LNCaP.
Notes: The role of endogenous cholesterol, macropinocytosis, clathrin, and clathrin-independent mechanisms was determined by prior treatment with methyl-β-cyclodextrin, amiloride, nystatin, and chlorpromazine respectively.
Abbreviations: PCL, polycaprolactone; MD, maltodextrin; Pos cont, positive control; MβCD, methyl-β-cyclodextrin; CPZ, chlorpromazine; Neg cont, negative control.

the drugs' bioavailability. Further, they present a solution to the stability and delivery of therapeutic macromolecules, which are generally unstable at physiological conditions and are also unable to cross cell membranes unassisted due to their large sizes. The efficiency of the PCL/MD nanocarriers for subcellular drug delivery in PCa was illustrated with coumarin-6 and FITC-BSA as a model small and large molecule, respectively. Coumarin-6 was used as a model small molecule due to its extreme hydrophobic nature that limits it bioavailability. Its highly fluorescent nature also allowed its intracellular tracking. Previous studies have shown that coumarin entrapped within nanocarriers has very low amounts released outside the cell; hence, the observed intracellular fluorescence correlates directly with the internalization of entrapped drug within the nanocarrier rather than the leaked free drug form.[39,49] Entrapment of the molecules within the PCL/MD resulted in a much higher intracellular drug content than the free non-encapsulated drug (Figure 5A). This higher efficiency was as a result of the internalization of the drug nanocarrier as demonstrated by the fluorescent images in Figure 5. This result was hence in agreement with previous studies where coumarin-6 dye showed very negligent uptake in treated cell lines.[50,51]

The rapid and efficient internalization of the nanocarrier observed possibly occurred as a result of the hydrophobic nature of the polymer employed and its moderately low-negative surface charge, as indicated by earlier studies.[17,18] Also, the cellular internalization of the nanocarriers was found to increase with increasing tumorigenic potential of the cell line. PC3 and DU145 showed a much faster rate and extent of internalization of PCL/MD than LNCaP; there was a significant ($P<0.05$) amount of cellular fluorescence obtained within a short time (5 minutes) with an increasing cytoplasmic and possible nuclear localization with time. This result was confirmed by fluorescence microscopic studies in PC3 cell lines. The rate of uptake, however, decreased with time due to possible saturation or a balance formed between cellular internalization and exocytosis, although moderate increase in intracellular drug content was observed after the initial rapid increase. A similar pattern was obtained in LNCaP, although the rate of internalization was slower and sustained for 2 hours, after which very little to no increase in uptake was observed (Figure 6). Oncogenic activation is usually associated with alterations in receptor-initiated signaling pathways, which lead to an increase in the uptake and metabolism of nutrients required to meet the bioenergetics demand of uncontrolled proliferation of cancer cells.[52,53] Overall, internalization was highest in PC3 followed by DU145 and LNCaP, respectively. This can be attributed to PC3's higher metabolic and energy demands required to meet its aggressive and highly proliferative nature.

The internalization of PCL/MD nanocarrier was further determined to be metabolically dependent in all the three PCa cell lines studied, although the role of metabolically-independent pathways cannot be discounted as demonstrated in previous reports.[54–56] Since endocytosis is an energy-dependent

mechanism, reduction of the incubation temperature from 37°C to 4°C caused a significant ($P<0.05$) decrease in the uptake in all three cell lines.[57–59] Several metabolic pathways have so far been identified to be involved in nanoparticle internalization. With each differing in its sorting or trafficking pathways, it is imperative for further understanding of the differences in endocytic mechanisms involved in the uptake of our PCL/MD nanocarrier in the three PCa cell lines. Our results demonstrated that endogenous cholesterol played a major role in the uptake of nanocarrier in PC3, DU145, and LNCaP. However, there were significant differences in the degree to which extraction of cholesterol by MβCD[30,31,34] affected the nanocarrier internalization in the different cell lines. Extraction of cholesterol in PC3 resulted in about 75%±4.53% decrease in cellular internalization, while a decrease of 64%±6.01% and 50%±4.50% was observed in LNCaP and DU145, respectively.

Macropinocytosis also showed involvement in the nanocarrier internalization in all three PCa cell lines. This endocytic pathway has been reported to be very critical in cancer cells, serving as a route for the intracellular transport of amino acids (proteins) required for the central carbon metabolic process.[60] It has been shown in an independent study that the overexpression of Ras protein, an oncogenic protein resulted in an increased cell proliferation that was concomitant with an increase in macropinocytosis.[61] Additionally, CIP and CME were all significantly involved in PCL/MD nanocarrier internalization in PC3 and DU145. Although, macropinocytosis and CIP were involved in PCL/MD internalization in LNCaP, inhibition of the CME had very little to no effect on nanocarrier uptake. This possibly may be due to its relatively higher AR expression, which has been reported to alter CME in LNCaP and PC3-AR cell lines.[25] CME is the main internalization pathway of macromolecules and plasma membrane constituents in most cell types; hence, any alteration in this pathway will have significant effect on the rate, extent of internalization, and tumor concentration of nanotherapeutics for the management of the early phase of PCa.

The multi-mechanism of PCL/MD internalization in PC3 may have accounted for the highly diffused and non-compartmentalized nature of internalized nanocarrier observed in the fluorescence microscopic images (Figure 7). Colocalization of some of the internalized nanocarrier with lysosomes after an hour of incubation can be attributed to entry via CME in PC3. Although this may be deleterious for molecules that are highly susceptible to proteolytic degradation, lysosomal colocalization can be further exploited for lysosomal targeting, delivery of enzymes for lysosomal storage diseases, and delivery of anticancer agents and prodrugs that require enzymatic cleavage. Earlier work by Thurn et al indicated that the uptake of titanium dioxide in PC3 was mediated by both CME and macropinocytosis,[55] while the uptake of double-walled carbon nanotubes was found to be by CME.[62] Furthermore, the uptake of PLGA nanoparticles in PC3 significantly decreased upon inhibition by the formation of clathrin-coated pits upon pretreatment with hypertonic growth medium.[63] Nonetheless, it will be erroneous for a direct comparison with these previous studies to be made due to the significant difference in internalization pathways for different nanocarriers, materials, surface charges, particle sizes, and even cell seeding density.

This study therefore serves as a first report of the possible impact of PCa heterogeneity and progression on the cellular internalization of a PCL-based nanocarrier. In order to identify the specific proteins involved in the internalization of these nanocarriers in PCa, the authors are currently looking at the effect of the expression of mutated endocytic proteins or their knock down with siRNA on the endocytic processes that they control. The role of AR expression on in vivo tumor concentrations of drug-loaded nanoparticles will also be investigated in the future.

Conclusion

Nanocarrier cellular uptake, internalization pathway, and intracellular fate have a direct impact on the efficiency of nanotherapeutic approaches for cancer management. Alterations in these pathways as a result of disease progression and heterogeneity may therefore alter the efficiency of nanomedicines. Using PCL/MD nanocarrier as a model, substantially higher intracellular drug concentration was obtained in all three PCa cell lines when compared to the free drug form. PCL/MD nanocarriers significantly increased intracellular drug concentration in LNCaP, DU145, and PC3. Nanocarrier cellular internalization was found to increase with aggressiveness of the cell line. The AUC for PC3 was 2- and 1.3-fold higher than that for LNCaP and DU145, respectively. Nanocarrier internalization in the more aggressive cell lines, PC3 and DU145, were mediated by all three classical endocytic pathways, ie, macropinocytosis, CIP, and CME. However, PCL/MD nanocarrier internalization in LNCaP was predominantly by CIP and macropinocytosis. PCL/MD nanocarriers were highly diffused subcellularly and non-compartmentalized due to the multi-mechanisms involved in their internalization. This study therefore indicates the possible impact of disease progression on nanocarrier

internalization and the need to factor these alterations in the design of nanocarrier dosage forms for the treatment of advance states of PCa.

Acknowledgment

The authors thank Cedar HA Boakye, Rosemary Amissah, and Peri Nagappan for their support and contribution.

Disclosure

The authors declare no conflicts of interest in this work.

References

1. Almouazen E, Bourgeois S, Boussaïd A, et al. Development of a nanoparticle-based system for the delivery of retinoic acid into macrophages. *Int J Pharm*. 2012;430(1–2):207–215.
2. Duncan R. The dawning era of polymer therapeutics. *Nat Rev Drug Discov*. 2003;2(5):347–360.
3. Peer D, Karp JM, Hong S, Farokhzad OC, Margalit R, Langer R. Nanocarriers as an emerging platform for cancer therapy. *Nat Nanotechnol*. 2007;2(12):751–760.
4. Davis ME, Chen ZG, Shin DM. Nanoparticle therapeutics: an emerging treatment modality for cancer. *Nat Rev Drug Discov*. 2008;7(9):771–782.
5. Mosqueira VC, Legrand P, Gulik A, et al. Relationship between complement activation, cellular uptake and surface physicochemical aspects of novel PEG-modified nanocapsules. *Biomaterials*. 2001;22(22):2967–2979.
6. Nowacek AS, Balkundi S, McMillan J, et al. Analyses of nanoformulated antiretroviral drug charge, size, shape and content for uptake, drug release and antiviral activities in human monocyte-derived macrophages. *J Control Release*. 2011;150(2):204–211.
7. Liu J, Bauer H, Callahan J, Kopecková P, Pan H, Kopecek J. Endocytic uptake of a large array of HPMA copolymers: elucidation into the dependence on the physicochemical characteristics. *J Control Release*. 2010;143(1):71–79.
8. Gratton SE, Ropp PA, Pohlhaus PD, et al. The effect of particle design on cellular internalization pathways. *Proc Natl Acad Sci U S A*. 2008;105(33):11613–11618.
9. Pangarkar C, Dinh A-T, Mitragotri S. Endocytic pathway rapidly delivers internalized molecules to lysosomes: an analysis of vesicle trafficking, clustering and mass transfer. *J Control Release*. 2012;162(1):76–83.
10. Kaplan J. Cell contact induces an increase in pinocytotic rate in cultured epithelial cells. *Nature*. 1976;263(5578):596–597.
11. Snijder B, Sacher R, Rämö P, Damm E-M, Liberali P, Pelkmans L. Population context determines cell-to-cell variability in endocytosis and virus infection. *Nature*. 2009;461(7263):520–523.
12. Barua S, Rege K. Cancer-cell-phenotype-dependent differential intracellular trafficking of unconjugated quantum dots. *Small*. 2009;5(3):370–376.
13. Woodruff MA, Hutmacher DW. The return of a forgotten polymer – polycaprolactone in the 21st century. *Prog Polym Sci*. 2010;35(10):1217–1256.
14. Sinha VR, Bansal K, Kaushik R, Kumria R, Trehan A. Poly-epsilon-caprolactone microspheres and nanospheres: an overview. *Int J Pharm*. 2004;278(1):1–23.
15. Williams JM, Adewunmi A, Schek RM, et al. Bone tissue engineering using polycaprolactone scaffolds fabricated via selective laser sintering. *Biomaterials*. 2005;26(23):4817–4827.
16. Jaiswal J, Kumar Gupta S, Kreuter J. Preparation of biodegradable cyclosporine nanoparticles by high-pressure emulsification-solvent evaporation process. *J Control Release*. 2004;96(1):169–178.
17. Dash TK, Konkimalla VB. Poly-ϵ-caprolactone based formulations for drug delivery and tissue engineering: a review. *J Control Release*. 2012;158(1):15–33.
18. Chawla JS, Amiji MM. Biodegradable poly(ε-caprolactone) nanoparticles for tumor-targeted delivery of tamoxifen. *Int J Pharm*. 2002;249(1–2):127–138.
19. Corveleyn S, Remon JP. Maltodextrins as lyoprotectants in the lyophilization of a model protein, LDH. *Pharm Res*. 1996;13(1):146–150.
20. Dekeyser PM, Corveleyn S, Demeester J, Remon J-P. Stabilization of fully active chymopapain by lyophilization. *Int J Pharm*. 1997;159(1):19–25.
21. Devineni D, Ezekwudo D, Palaniappan R. Formulation of maltodextrin entrapped in polycaprolactone microparticles for protein and vaccine delivery: effect of size determining formulation process variables of microparticles on the hydrodynamic diameter of BSA. *J Microencapsul*. 2007;24(4):358–370.
22. Boyd LK, Mao X, Lu Y-J. The complexity of prostate cancer: genomic alterations and heterogeneity. *Nat Rev Urol*. 2012;9(11):652–664.
23. LaTulippe E, Satagopan J, Smith A, et al. Comprehensive gene expression analysis of prostate cancer reveals distinct transcriptional programs associated with metastatic disease. *Cancer Res*. 2002;62(15):4499–4506.
24. Apodaca G. Endocytic traffic in polarized epithelial cells: role of the actin and microtubule cytoskeleton. *Traffic*. 2001;2(3):149–159.
25. Bonaccorsi L, Nosi D, Muratori M, Formigli L, Forti G, Baldi E. Altered endocytosis of epidermal growth factor receptor in androgen receptor positive prostate cancer cell lines. *J Mol Endocrinol*. 2007;38(1–2):51–66.
26. Tilley WD, Wilson CM, Marcelli M, McPhaul MJ. Androgen receptor gene expression in human prostate carcinoma cell lines. *Cancer Res*. 1990;50(17):5382–5386.
27. Nemeth JA, Harb JF, Barroso U, He Z, Grignon DJ, Cher ML. Severe combined immunodeficient-hu model of human prostate cancer metastasis to human bone. *Cancer Res*. 1999;59(8):1987–1993.
28. Subtil A, Gaidarov I, Kobylarz K, Lampson MA, Keen JH, McGraw TE. Acute cholesterol depletion inhibits clathrin-coated pit budding. *Proc Natl Acad Sci U S A*. 1999;96(12):6775–6780.
29. Nabi IR, Le PU. Caveolae/raft-dependent endocytosis. *J Cell Biol*. 2003;161(4):673–677.
30. Imelli N, Meier O, Boucke K, Hemmi S, Greber UF. Cholesterol is required for endocytosis and endosomal escape of adenovirus type 2. *J Virol*. 2004;78(6):3089–3098.
31. Rodal SK, Skretting G, Garred O, Vilhardt F, van Deurs B, Sandvig K. Extraction of cholesterol with methyl-beta-cyclodextrin perturbs formation of clathrin-coated endocytic vesicles. *Mol Biol Cell*. 1999;10(4):961–974.
32. Wang LH, Rothberg KG, Anderson RG. Mis-assembly of clathrin lattices on endosomes reveals a regulatory switch for coated pit formation. *J Cell Biol*. 1993;123(5):1107–1117.
33. Ivanov AI. Pharmacological inhibition of endocytic pathways: is it specific enough to be useful? *Methods Mol Biol*. 2008;440:15–33.
34. Iversen T-G, Skotland T, Sandvig K. Endocytosis and intracellular transport of nanoparticles: present knowledge and need for future studies. *Nano Today*. 2011;6(2):176–185.
35. Sahay G, Alakhova DY, Kabanov AV. Endocytosis of nanomedicines. *J Control Release*. 2010;145(3):182–195.
36. Koivusalo M, Welch C, Hayashi H, et al. Amiloride inhibits macropinocytosis by lowering submembranous pH and preventing Rac1 and Cdc42 signaling. *J Cell Biol*. 2010;188(4):547–563.
37. Kälin S, Amstutz B, Gastaldelli M, et al. Macropinocytotic uptake and infection of human epithelial cells with species B2 adenovirus type 35. *J Virol*. 2010;84(10):5336–5350.
38. Lamprecht A, Ubrich N, Hombreiro Pérez M, Lehr C, Hoffman M, Maincent P. Influences of process parameters on nanoparticle preparation performed by a double emulsion pressure homogenization technique. *Int J Pharm*. 2000;196(2):177–182.

39. Win KY, Feng S-S. Effects of particle size and surface coating on cellular uptake of polymeric nanoparticles for oral delivery of anticancer drugs. *Biomaterials*. 2005;26(15):2713–2722.
40. Jin H, Heller DA, Sharma R, Strano MS. Size-dependent cellular uptake and expulsion of single-walled carbon nanotubes: single particle tracking and a generic uptake model for nanoparticles. *ACS Nano*. 2009;3(1):149–158.
41. Zhang S, Li J, Lykotrafitis G, Bao G, Suresh S. Size-dependent endocytosis of nanoparticles. *Adv Mater*. 2009;21:419–424.
42. Maeda H. Tumor-selective delivery of macromolecular drugs via the EPR effect: background and future prospects. *Bioconjug Chem*. 2010;21(5):797–802.
43. Awasthi VD, Garcia D, Goins BA, Phillips WT. Circulation and biodistribution profiles of long-circulating PEG-liposomes of various sizes in rabbits. *Int J Pharm*. 2003;253(1–2):121–132.
44. Wang X, Wang Y, Wei K, Zhao N, Zhang S, Chen J. Drug distribution within poly(ε-caprolactone) microspheres and in vitro release. *J Mater Process Technol*. 2009;209(1):348–354.
45. Yang YY, Chung TS, Ng NP. Morphology, drug distribution, and in vitro release profiles of biodegradable polymeric microspheres containing protein fabricated by double-emulsion solvent extraction/evaporation method. *Biomaterials*. 2001;22(3):231–241.
46. Dubernet C. Thermoanalysis of microspheres. *Thermochim Acta*. 1995;248:259–269.
47. Elnaggar YSR, El-Massik MA, Abdallah OY, Ebian AER. Maltodextrin: a novel excipient used in sugar-based orally disintegrating tablets and phase transition process. *AAPS Pharm Sci Tech*. 2010;11(2):645–651.
48. Myers SL, Shively ML. Solid-state emulsions: the effects of maltodextrin on microcrystalline aging. *Pharm Res*. 1993;10(9):1389–1391.
49. Eley JG, Pujari VD, McLane J. Poly(lactide-co-glycolide) nanoparticles containing coumarin-6 for suppository delivery: in vitro release profile and in vivo tissue distribution. *Drug Deliv*. 2004;11(4):255–261.
50. Roger E, Kalscheuer S, Kirtane A, et al. Folic acid functionalized nanoparticles for enhanced oral drug delivery. *Mol Pharm*. 2012;9(7):6–13.
51. Dong Y, Feng S-S. Poly(d,l-lactide-co-glycolide)/montmorillonite nanoparticles for oral delivery of anticancer drugs. *Biomaterials*. 2005;26(30):6068–6076.
52. Vander Heiden MG, Cantley LC, Thompson CB. Understanding the Warburg effect: the metabolic requirements of cell proliferation. *Science*. 2009;324(5930):1029–1033.
53. DeBerardinis RJ, Lum JJ, Hatzivassiliou G, Thompson CB. The biology of cancer: metabolic reprogramming fuels cell growth and proliferation. *Cell Metab*. 2008;7(1):11–20.
54. Verma A, Uzun O, Hu Y, et al. Surface-structure-regulated cell-membrane penetration by monolayer-protected nanoparticles. *Nat Mater*. 2013;12(4):376–376.
55. Thurn KT, Arora H, Paunesku T, et al. Endocytosis of titanium dioxide nanoparticles in prostate cancer PC-3M cells. *Nanomedicine*. 2011;7(2):123–130.
56. Paillard A, Hindré F, Vignes-Colombeix C, Benoit J-P, Garcion E. The importance of endo-lysosomal escape with lipid nanocapsules for drug subcellular bioavailability. *Biomaterials*. 2010;31(29):7542–7554.
57. Brickman MJ, Cook JM, Balber AE. Low temperature reversibly inhibits transport from tubular endosomes to a perinuclear, acidic compartment in African trypanosomes. *J Cell Sci*. 1995;108(1):3611–3621.
58. Steinman RM, Mellman IS, Muller WA, Cohn ZA. Endocytosis and the recycling of plasma membrane. *J Cell Biol*. 1983;96(1):1–27.
59. Tomoda H, Kishimoto Y, Lee YC. Temperature effect on endocytosis and exocytosis by rabbit alveolar macrophages. *J Biol Chem*. 1989;264(26):15445–15450.
60. Trajkovska M. Macropinocytosis supports cancer cell proliferation. *Nat Cell Biol*. 2013;15(7):729–729.
61. Commisso C, Davidson SM, Soydaner-Azeloglu RG, et al. Macropinocytosis of protein is an amino acid supply route in Ras-transformed cells. *Nature*. 2013;497(7451):633–637.
62. Neves V, Gerondopoulos A, Tîlmaciu C, et al. Cellular localization, accumulation and trafficking of DWNTs in human prostate cancer cells. *Nano Res*. 2012;5(4):223–234.
63. Panyam J, Zhou W-Z, Prabha S, Sahoo SK, Labhasetwar V. Rapid endo-lysosomal escape of poly(DL-lactide-co-glycolide) nanoparticles: implications for drug and gene delivery. *FASEB J*. 2002;16(10):1217–1226.

Supplementary materials

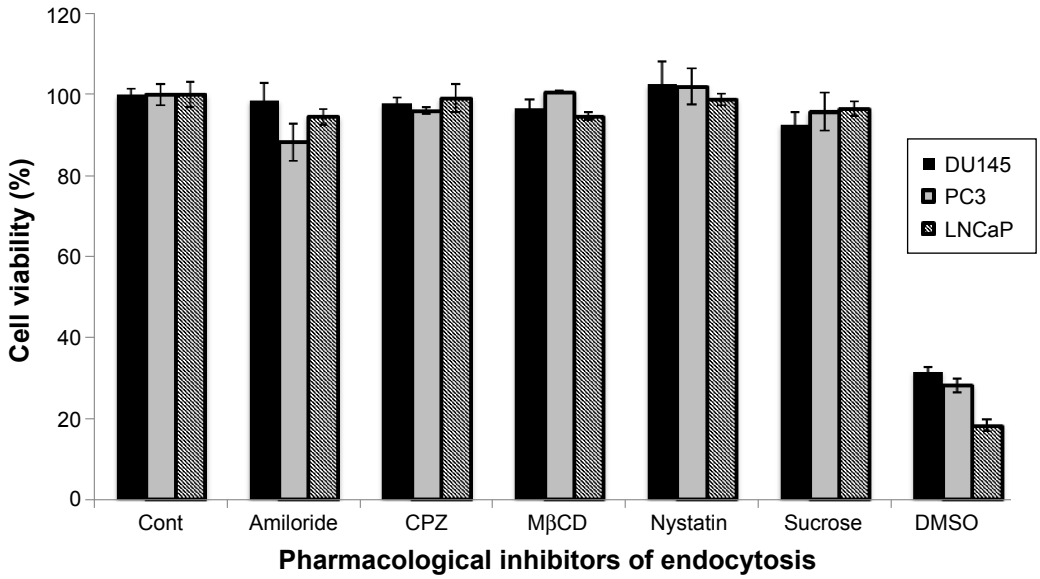

Figure S1 Effect of pharmacological inhibitors on viability of prostate cell lines studied.
Abbreviations: Cont, control; CPZ, chlorpromazine; MβCD, methyl-β-cyclodextrin; DMSO, dimethyl sulfoxide.

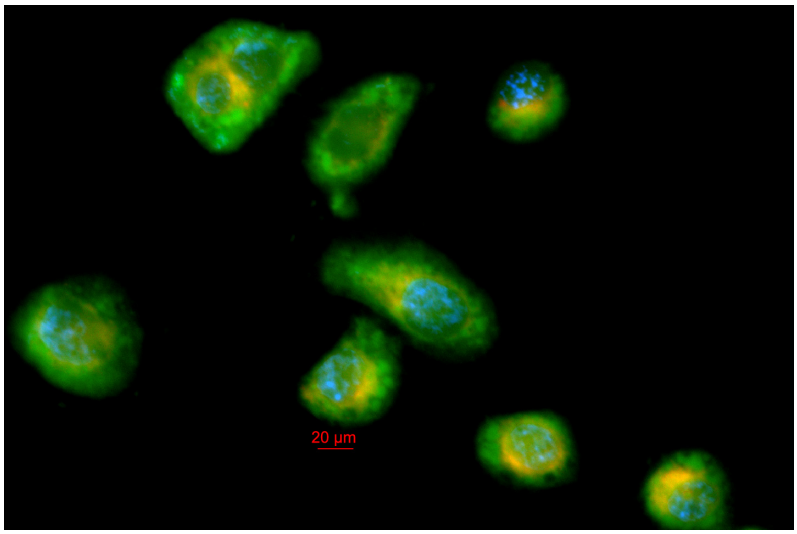

Figure S2 Image showing nanocarrier colocalization with acidic organelles.

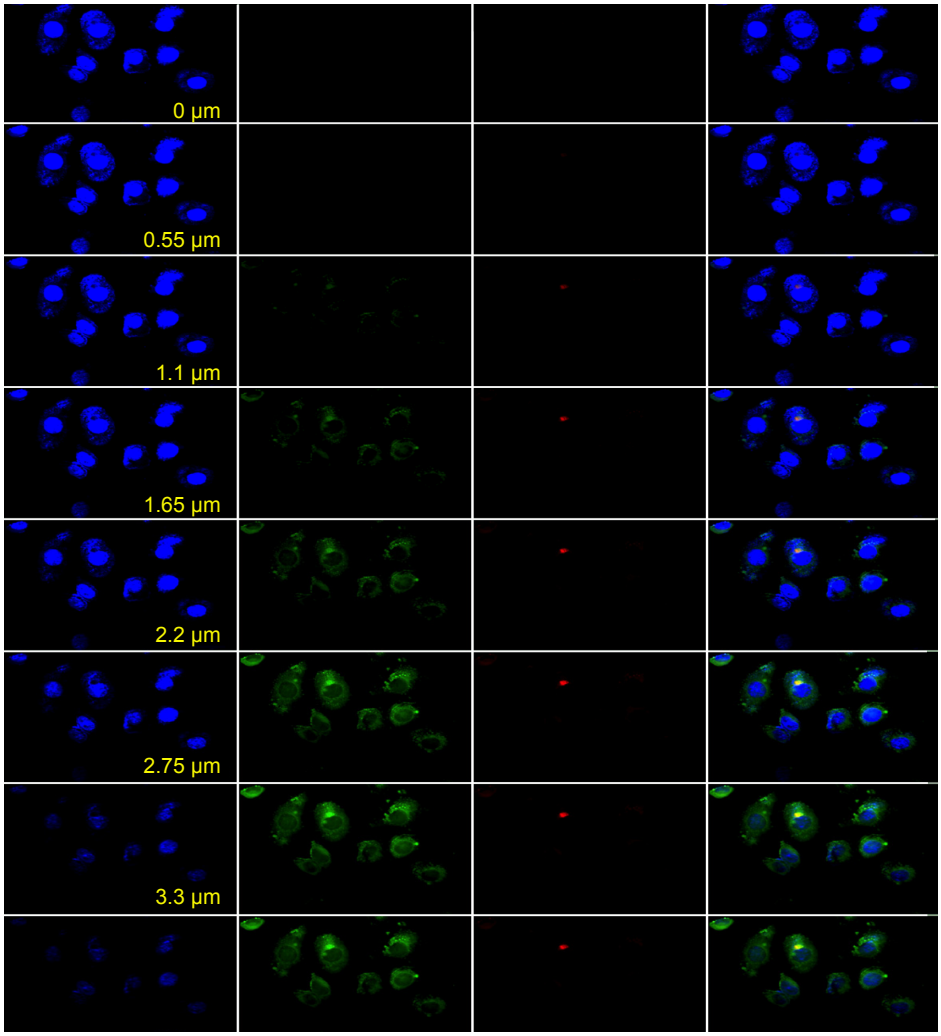

Figure S3 Z-stacked ApoTome images showing intracellular localization of nanocarrier.